ISSN 1990-3413, Astrophysical Bulletin, 2017, Vol. 72, No. 2, pp. 184–190. © Pleiades Publishing, Ltd., 2017.
Original Russian Text © N.V. Borisov, M.M. Gabdeev, V.V. Shimansky, N.A. Katysheva, S.Yu. Shugarov, 2017, published in Astrofizicheskii Byulleten', 2017, Vol. 72, No. 2, pp. 204–211.

Spectral and Photometric Studies of Polar CRTS CSS 130604 J 215427+155714

N. V. Borisov[1], M. M. Gabdeev[1*], V. V. Shimansky[2], N. A. Katysheva[3], and S. Yu. Shugarov[3,4]

[1]*Special Astrophysical Observatory, Russian Academy of Sciences, Nizhnii Arkhyz, 369167 Russia*
[2]*Kazan (Volga region) Federal University, Kazan, 420008 Russia*
[3]*Sternberg Astronomical Institute, Moscow State University, Moscow, 119991 Russia*
[4]*Astronomical Institute of the Slovak Academy of Sciences, Tatranska Lomnica, 05960 Slovakia*

Received September 21, 2016; in final form, February 2, 2017

Abstract—We present the results of spectroscopic and photometric studies of a new polar CRTS CSS 130604 J 215427+155714, conducted at the telescopes of the SAO RAS. Analysis of the photometric series of observations allowed to clarify the orbital period of the system, $P_o = 0\overset{\mathrm{d}}{.}0672879$ (± 0.0000003). We build radial velocity curves and trace the intensity variations in the Hβ and Hγ hydrogen lines and He II λ 4686 Å ionized helium line. Based on the Hβ and He II lines we build Doppler maps. It is shown that the line formation region is localized near the Lagrange point. The following parameter estimates of the system are obtained: $M_1 = 0.83 \pm 0.10 M_\odot$, $M_2 = 0.15 \pm 0.01 M_\odot$, $q = M_2/M_1 = 0.18 \pm 0.03$, $i = 53^\circ \pm 5^\circ$. Based on the results of spectral, photometric and previously published polarimetric observations the possible geometric model of the system is discussed.

DOI: 10.1134/S1990341317020092

Key words: *novae, cataclysmic variables—stars: individual: CRTS CSS 130604 J 215427+155714—methods: polarization*

1. INTRODUCTION

The polar CRTS CSS 130604 J 215427+155714 (further referred to as CSS 130604) we study has been for the first time discovered by Szkody et al. [1] in the paper, devoted to the search for the cataclysmic variables from the SDSS [2], CRTS [3] and vsnet alert[1] catalogs. The amplitude of its orbital brightness variability up to $1\overset{\mathrm{m}}{.}5$. The spectrum revealed a strong line of ionized helium He II λ 4686 Å. The half-amplitude of radial velocity variation measured based on it reached 300 km s^{-1} with the orbital period of $P_o = 96.9$ min. Polarimetric observations presented in the paper [4] showed that the object has a strong circular polarization in the V-band up to -22% not changing the polarization sign during the orbital period. This allowed to classify CSS 130604 as a polar.

Polars are a not very numerous subclass of nova-like cataclysmic variables pertaining to short-period close binary systems (CBS). In such systems, a white dwarf (the main component) has a strong magnetic field (10–100 MG), which leads to the implementation of the regime of channeled accretion to its magnetic poles. It is believed that in such CBSs the Alfven radius exceeds the dimensions of the system. Instead of the accretion disk, magnetic lines of force form a stream of outflowing material, which falls in the regions of magnetic poles of the white dwarf. The optical radiation of polars is strongly polarized, in some cases up to 30–40%, since it has cyclotron nature. The observations reveal a high degree of photometric and spectral variability on the time scale from seconds to several years, sometimes it is manifested in the form of flare activity. The radiation of polars is registered in a wide range of the electromagnetic spectrum: from X-ray to infrared.

Note that the observational manifestations of component interaction are confirmed not only by the accretion processes, but also by the effects of re-emission of ultraviolet and X-ray radiation in the stream of outflowing matter and on the surface of the secondary component.

This paper continues the cycle of studies of polars [4–6], devoted to finding the main parameters of the investigated systems from the spectroscopic, photometric and polarimetric data obtained at the

*E-mail: crucifer.troll@gmail.ru

[1] http://ooruri.kusastro.kyoto-u.ac.jp/pipermail/vsnet-alert/

telescopes of the Special Astrophysical Observatory of the Russian Academy of Sciences (SAO RAS).

2. OBSERVATIONS

2.1. Photometry

Photometric observations of CSS 130604 were conducted at the 1-m Zeiss-1000 telescope of the SAO RAS in November 2014 and August 2015. A regular photometer with a set of the Johnson-Cousins system B, V, R_c broadband filters and a EEV 42-40 CCD detector (2048×2048 pixels sized $13.5 \times 13.5 \mu$m) with nitrogen cooling were used. Figure 1 presents the field around the investigated object with reference stars marked. The information about them is presented in Table 1.

2.2. Spectroscopy

Spectroscopy was performed at the SAO RAS 6-m BTA telescope with the SCORPIO focal reducer [7] and the nitrogen-cooled EEV 42-40 CCD detector (2048×2048 pixels). The observations were carried out on November 22, 2014 at the average atmosphere transparency and the seeing of about $2''.5$. A three-dimensional holographic grating was used with 1200 strokes mm^{-1} (VPHG1200G) and a $1''$-wide slit. We obtained 21 spectral image in the range of 3900–5700 Å with a resolution of 5.5 Å and equal exposures of 300 s. To calibrate wavelengths, we used a lamp with He-Ne-Ar filling, and the star BD 28+4211 as a spectrophotometric standard [8]. Reduction was carried out in the IDL environment[2] within the standard procedure.

3. ANALYSIS OF OBSERVATIONAL DATA

3.1. Photometry

Based on the results of photometric observations in the R_c-band, we have carried out a harmonic analysis of the time series. The Lafler-Kinman method [9] was applied, implemented in the Goranskij's EFFECT code[3]. The ephemeris of the object was refined, while the zero phase selected was the time of minimal system brightness:

$$\begin{aligned} \mathrm{HJD} &= 2456987^{\mathrm{d}}.189\,(\pm 0.001) \quad (1) \\ &+ 0^{\mathrm{d}}.0672879\,(\pm 0.0000003)\,E. \end{aligned}$$

The ephemeris found was used to plot the light curves. They have a quasi-sinusoidal shape with the duration of maximum and minimum $\delta\phi = 0.3$ and $\delta\phi = 0.2$, respectively. The shape of the light curves in the B, V, R_c filters is similar to (Fig. 2). The magnitude at the brightness maximum in the following bands amounted to: $V = 16^{\mathrm{m}}.45 \pm 0.03$, $R_c = 16^{\mathrm{m}}.77 \pm 0.03$ and $B = 17^{\mathrm{m}}.90 \pm 0.08$. The brightness variation amplitude in the R_c-band is approximately $1^{\mathrm{m}}.5$. This coincides with the result in the V-band presented in the paper [4]. The average brightness of the system in the R_c-band in November 2014 is equal to its average brightness according to the observations in August 2015.

3.2. Spectroscopy

In the spectra of the investigated object we observe intensive emission hydrogen lines of the Balmer series, neutral He I and ionized He II helium (Fig. 3), while in the phases of brightness maximum the cyclotron radiation line is also visible. It should be noted that the intensities of the He II λ 4686 Å and Hβ lines are almost identical, which is typical to the polars [10, 11].

The line intensity varies with orbital period in antiphase with the light curve (see Fig. 4). We can conclude from their comparative analysis that the emission line formation region is localized near the Lagrange point. Radial velocities from the emission line peaks were measured by the cross-correlation method. The results of radial-velocity measurements and their sinusoidal approximation are shown in Figs. **??**. The obtained values of half-amplitudes from the Hγ, Hβ and He II λ 4686 Å lines amounted to 276 ± 23, 317 ± 21 and 335 ± 11 km s^{-1}, respectively. As a rule, we observe in polars an increase in the radial velocity amplitude with increasing excitation potential of the lines under study. However, in the case of CSS 130604, insignificant differences in half-amplitude are due to the angle of inclination of the system's orbital plane to the line of sight. Note that the obtained set of amplitudes does not contradict the model of line formation given channeled accretion.

Doppler mapping was done based on the Hβ and He II λ 4686 Å line profiles with the aid of Spruit's Dopmap program package, implementing the method of entropy minimization [12]. Note that the Doppler maps are reconstructed in the velocity plane, where the X axis is directed from the white dwarf to the red dwarf, and the Y axis—along the orbital motion of the red dwarf. Unfortunately, the signal-to-noise ratio of the Hγ line turned out to be inadequate for the correct use of the method. According to the constructed Doppler maps (Fig. 6), there is no disk accretion, while the line formation region is located near the Lagrange point and covers the beginning of the jet of the outflowing matter.

[2] http://www.ittvis.com/idl

[3] http://www.vgoranskij.net/software/

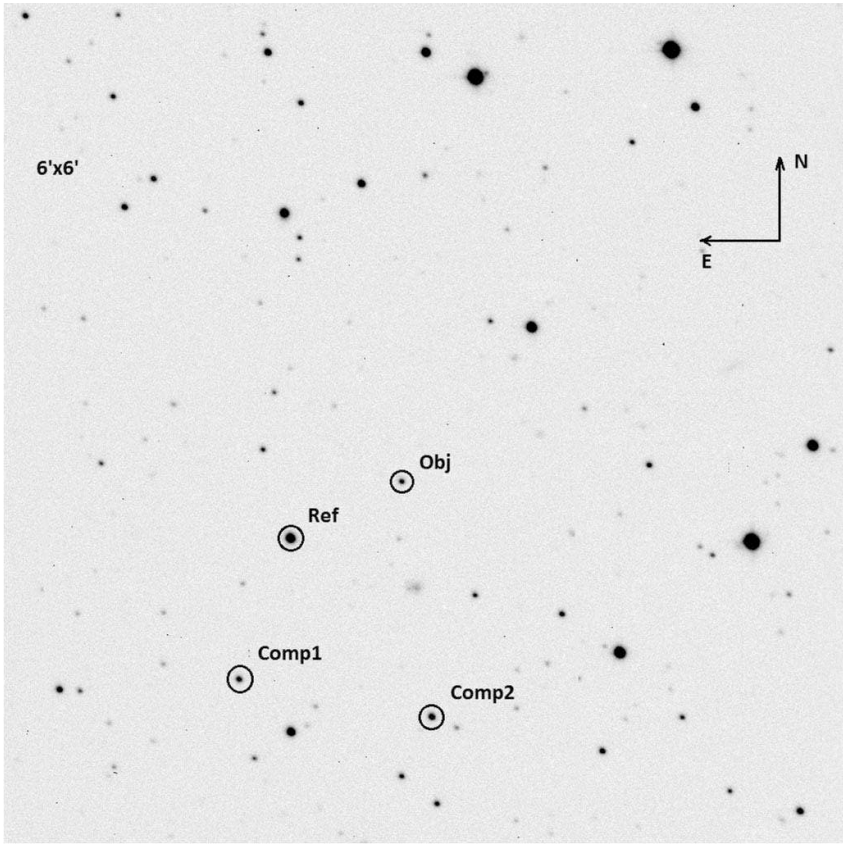

Fig. 1. The image of the object's vicinity with the secondary standard and comparison stars marked.

Table 1. Information about the reference stars

ID	α, hh:mm:ss.ss	δ, dd:mm:ss.ss	R_c, mag	B, mag	V, mag
Ref	21:54:31.32	+15:56:45.5	14.90 ± 0.01	16.67 ± 0.01	14.61 ± 0.01
Comp1	21:54:33.33	+15:55:31.5	16.70 ± 0.02	18.17 ± 0.05	16.27 ± 0.02
Comp2	21:54:36.49	+15:55:09.7	16.27 ± 0.02	19.5 ± 0.1	16.74 ± 0.02

3.3. System Parameters

We have estimated the component masses and the inclination of the system. Using the semi-empirical period–mass dependences [13, 14], we imposed restrictions on the mass of the red dwarf 0.11–0.16 $M_\odot$. To determine the mass function of the white dwarf, we used the following formula:

$$F(M_1) = 10385 \times 10^{-11} \left(1 - e^2\right)^{3/2} K_2^3 P_o, \quad (2)$$

where e is the eccentricity of the orbit, P_o is the orbital period, K_2 is the half-amplitude of radial velocities of the secondary component center of mass. The calculation was carried out for the Hβ line, since the measurements for it have the greatest accuracy, and the region of its formation is located near the L_1 point. The obtained estimate was corrected for the difference between the center of mass values of the red dwarf and the hot spot on its surface. The method of calculation of the corresponding ΔK_2 correction is described in detail in Section 5 of paper [5]. Its use for CSS130604 has shown that $\Delta K_2 = 31 \pm 3$ km s^{-1} with a weak dependence on the parameters of the system. As a result, the half-amplitude of the center of mass of the secondary component amounted to $K_2 = 348 \pm 21$ km s^{-1}. It should be noted that in the case of the object CSS 130604 a refinement of the orbital motion velocity of the secondary component only affects the system's angle of inclination. Thus, the mass function of the white dwarf calculated by the formula (2) at $e = 0$ amounts to $F(M_1) = 0.29$.

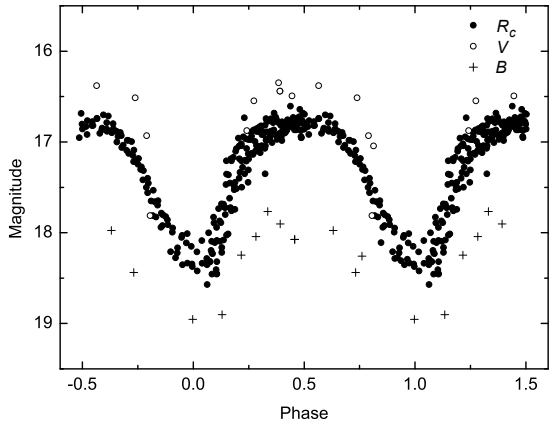

Fig. 2. The system brightness variations in the BVR_c-band with the phase of the orbital period in November 2014 and August 2015. The errors of brightness estimates did not exceed $0^{\rm m}.1$ (smaller than the size of the symbols).

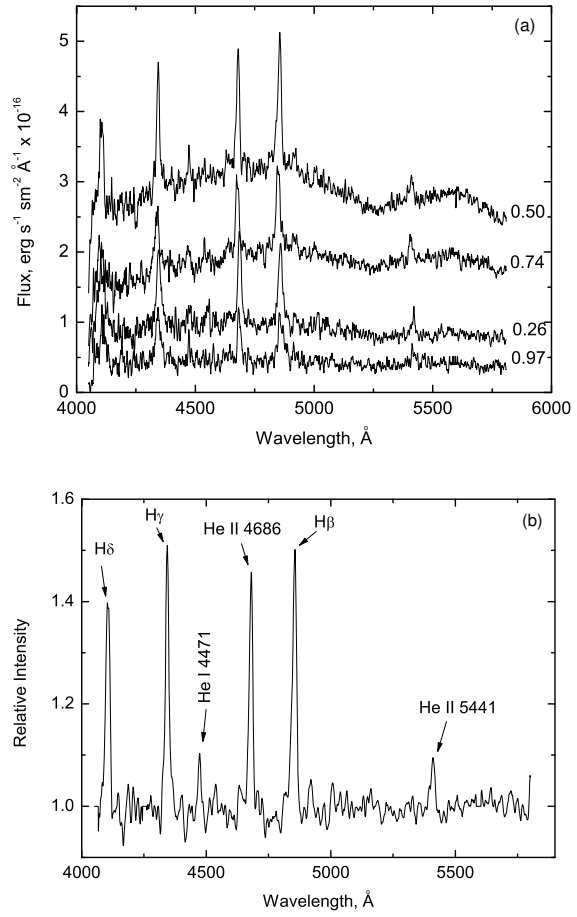

Fig. 3. Variations in the shape of the object spectrum in absolute magnitudes with the orbital period phase (a). The total spectrum of the object normalized to the continuum with the main emission lines marked (b).

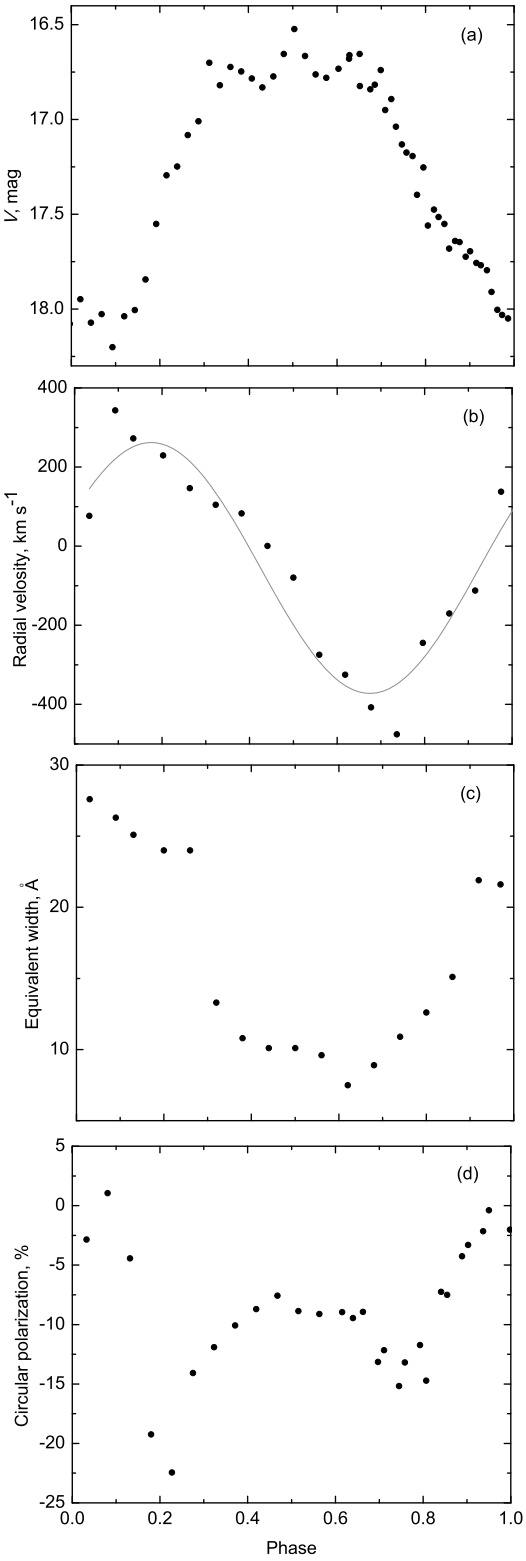

Fig. 4. Variations of the characteristic magnitudes during the orbital period: (a) the light curve in the V-band, (b) the radial velocity curve, measured from the Hβ line, and its approximation by a sinusoid, (c) the variation of the equivalent Hβ line width, (d) the circular polarization curve in the V-band.

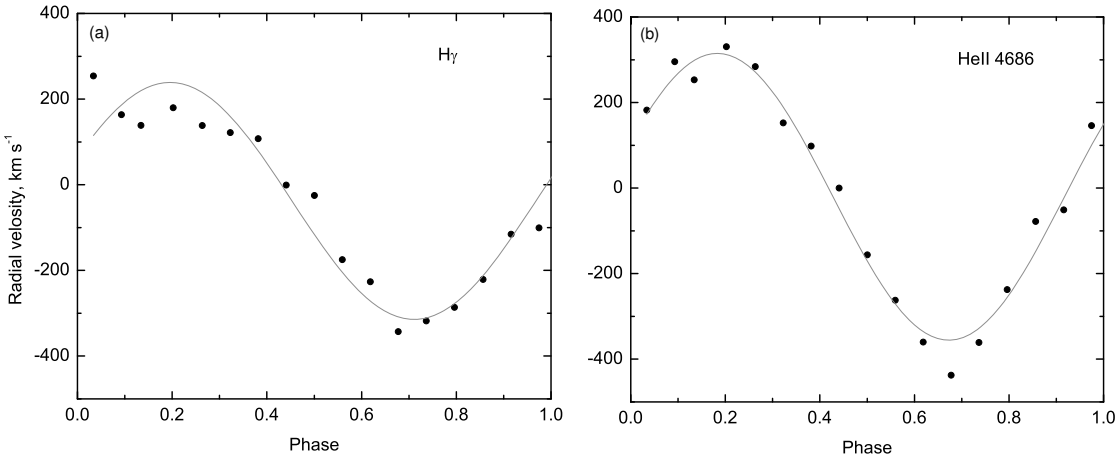

Fig. 5. Radial velocity curves from the Hγ (a) and He II λ 4686 Å (b) lines.

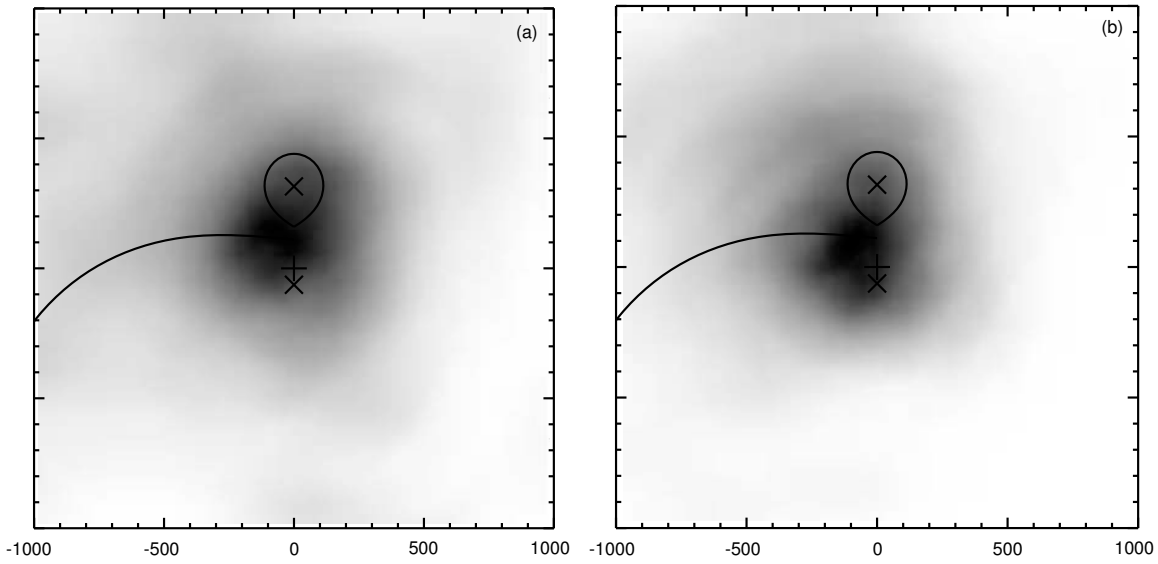

Fig. 6. Doppler maps constructed from the Hβ (a) and He II λ 4686 Å lines (b). The maps contain the following marks: "x" stands for the centers of mass of the white and red dwarfs, "+" is the center of mass of the binary, and also the Roche lobe of the secondary component and the trajectory of the matter infall outflow with the Keplerian velocities.

At the same time,

$$F(M_1) = \frac{M_1^3 \sin^3(i)}{(M_1 + M_2)^2}, \qquad (3)$$

where M_1, M_2 are the masses of the components, i is the angle of inclination of the orbital plane to the observer's line of sight. And, varying the mass of the white dwarf, for various angles of inclination of the system we found the parameters at which the mass function, determined from the formula (3) within the specified error coincided with the estimate $F(M_1) = 0.29 \pm 0.002$.

The upper boundary of the angle of inclination is $i \sim 75°$, since in the system there is neither a partial, nor a total eclipse (see the discussion). The minimum angle of inclination $i \sim 40°$ is limited by the Chandrasekhar limit (Fig. 7). Further on, based on the evolutionary tracks of cool stars of the Main Sequence [15] the values of the radius of the red dwarf were found $R_2 = 0.13$, 0.16 and 0.18 $M_\odot$ for three masses $M_2 = 0.11$, 0.14 and 0.16 $M_\odot$ respectively, with the chemical composition close to solar. Assuming that the Roche lobe radius R_{L2} is enclosed in the range of $1.05R_2 < R_{L2} < 1.09R_2$, we can obtain a mass estimate of the white dwarf. To this end, we calculated the values of R_{L2} for different values of the component mass ratio q using Eggleton's for-

Table 2. System parameter estimation

$M_2/M_\odot$	$R_2/R_\odot$	q	$M_1/M_\odot$	$R_{L2}/R_\odot$	R_2/R_{L2}	i, deg
0.11	0.132	0.09	1.22	0.144	1.088	41
0.14	0.159	0.15	0.93	0.169	1.063	48
0.14	0.159	0.16	0.88	0.173	1.085	50
0.16	0.178	0.21	0.76	0.189	1.063	56
0.16	0.178	0.22	0.73	0.192	1.079	58

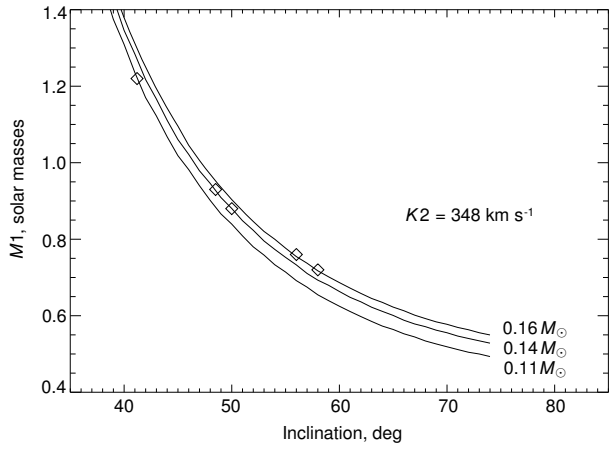

Fig. 7. The white dwarf mass varying the angle of the system inclination at the given mass and rotation velocity of the red dwarf. Diamonds indicate the values, obtained by comparing the radius of the secondary component with the Roche lobe radius (see Table 2).

mula [16]

$$R_{L2} = \frac{0.49q^{2/3}}{0.6q^{2/3} + \ln(1+q^{1/3})}, \quad 0 < q < \infty,$$

and compared them to the previously obtained red dwarf radii R_2. The results are presented in Table 2.

Discarding the mass estimate $M_2 = 0.11M_\odot$ as the least plausible, we obtain the following mean values: $M_1 = 0.83 \pm 0.10M_\odot$, $q = 0.18 \pm 0.03$, $i = 53^\circ \pm 5^\circ$. These parameters were used for the schematic representation of the system components at the Doppler maps, shown in Fig. 6.

4. DISCUSSION

We have conducted the spectroscopic and photometric observations for a detailed examination of the CSS 130604 object. The materials on its polarimetry and photometry from our paper [4] are also included in the investigation. A refined ephemeris (1) was obtained using all the data.

When analyzing the data obtained, we found it very important to take in the results of an earlier study of eclipsing polars, such as CRTS CSS 081231 J 071126+440405 [5] and BS Tri [17]. In eclipsing systems the position of components at different phases of orbital motion can be determined with a high confidence value. Eclipse occurs due to the occultation of the accretion region, located on the visible side of the white dwarf, by the red dwarf and, as a rule, falls on the maximum of the light curve.

The radial velocity of the emission line formation region on the surface of the secondary component at the time of the eclipse phase is equal to the gamma-velocity (the projection on the observer's line of sight is equal to 0) at the transition from negative to positive values (see, for example, Fig. 10 from [5]).

In the CSS 130604 system, on the contrary, at the time when the red dwarf is closer to the observer, the brightness is minimal, and the emission lines are the most intense. The circular polarization curve has two extrema, coinciding with the extrema of radial velocities: at phases 0.25 and 0.75, -23% and -13%, respectively, and two plateaus with the average values of -2.5% at the phases 0.95-0.1 and -8% at the phases 0.4–0.6.

With these features in mind, the following version of the geometric model of the system is possible. As noted above, the inclination of the system is close to 50°. Orientation of the white dwarf magnetic axis is such that the accretion region is always in the observer's field of view. This is confirmed by the invariance of the sign of circular polarization. The brightness minimum is observed at the time of self-occultation of the region where the continuum forms, when the cold part closes the hotter part. The radiation circular polarization maximum is achieved when the angle between the magnetic axis and the line of sight is 90° at phase 0.25. The same effect, but to a smaller extent is reiterated at phase 0.75. At the phases of about 0.5 the base of the accretion column is not closed and is most accessible to observations. As a result, a broad maximum is formed on the light curve, and the angle of inclination of the magnetic axis practically does not change. The emission line formation region, related with the stream of matter outflowing through the Lagrange point is also always

in the observer's field of view. A reduction of the equivalent line widths at the time of the peak brightness is due to an increase in the level of the continuum, which is a typical feature of emission in polars.

5. CONCLUSION

In the framework of a long-term program for the search and study of polars, we have conducted a complex analysis of observations of the polar CRTS CSS 130604 J215427+155714. According to the photometric data, the orbital period of the system was determined as $P_o = 0\overset{\mathrm{d}}{.}0672879\,(\pm 0.0000003)$. The observed spectra have the form characteristic of cataclysmic variables with channeled accretion. Radial velocities of the object were measured from the H I and He II emission lines, and the phase curves of the variation of their equivalent widths and Doppler tomography maps were built. It has been shown that the region of line formation is located near the Lagrange point. Therefore, the half-amplitude of the Hβ line radial velocity was used to estimate the masses of the system components ($M_1 = 0.83 \pm 0.10\ M_\odot$, $M_2 = 0.15 \pm 0.01\ M_\odot$, $q = 0.18 \pm 0.03$, $i = 53^\circ \pm 5^\circ$). Based on the analysis of the data obtained, including the polarimetric data, a geometric model of the system is proposed. Tables with measurements of the system brightness and radial velocities of different lines are available at `https://www.sao.ru/hq/lon/results.html`.

ACKNOWLEDGMENTS

The observations at the 6-meter BTA telescope are conducted with the financial support of the Ministry of Education and Science of the Russian Federation (Agreement No. 14.619.21.0004, project identifier RFMEFI61914X0004). The reduction of the observational data was carried out with the financial support of the Russian Science Foundation (RNF 14-50-00043), and the theoretical modeling—with the support of the Russian Foundation for Basic Research (RFFI 15-42-02573-a and 16-32-50200). N. A. Katysheva and S. Yu. Shugarov are grateful for the presidential grant Leading Scientific School (NSh-7690.2016.2). S. Yu. Shugarov also expresses gratitude to the VEGA Agency for the support by the grant No. 2/0002/13 and grant APVV-15-0458.

REFERENCES

1. P. Szkody, M. E. Everett, S. B. Howell, et al., Astron. J. **148**, 63 (2014).
2. D. G. York, J. Adelman, J. E. Anderson, Jr., et al., Astron. J. **120**, 1579 (2000).
3. A. J. Drake, S. G. Djorgovski, A. Mahabal, et al., Astrophys. J. **696**, 870 (2009).
4. N. V. Borisov, M. M. Gabdeev, and V. L. Afanasiev, Astrophysical Bulletin **71**, 95 (2016).
5. N. V. Borisov, M. M. Gabdeev, V. V. Shimansky, et al., Astrophysical Bulletin **71**, 101 (2016).
6. M. M. Gabdeev, Astrophysical Bulletin **70**, 460 (2015).
7. V. L. Afanasiev and A. V. Moiseev, Astronomy Letters **31**, 194 (2005).
8. R. C. Bohlin,Bull. Amer. Astron. Soc. **28**, 910 (1996).
9. J. Lafler and T. D. Kinman, Astrophys. J. Suppl. **11**, 216 (1965).
10. N. F. Voikhanskaya, Soviet Astron. Lett. **13**, 250 (1987).
11. J. Patterson, Publ. Astron. Soc. Pacific **106**, 209 (1994).
12. H. C. Spruit, arXiv:astro-ph/9806141 (1998).
13. S. B. Howell, L. A. Nelson, and S. Rappaport, Astrophys. J. **550**, 897 (2001).
14. C. Knigge, Monthly Notices Royal Astron. Soc. **373**, 484 (2006).
15. L. Girardi, A. Bressan, G. Bertelli, and C. Chiosi, Astron. and Astrophys. Suppl. **141**, 371 (2000).
16. P. P. Eggleton, Astrophys. J. **268**, 368 (1983).
17. N. V. Borisov, M. M. Gabdeev, V. V. Shimansky, et al., Astronomy Letters **41**, 646 (2015).

Translated by A. Zyazeva